HYPERSPECTRAL REMOTE SENSING IN LONG VALLEY CALDERA: ISSUES OF SCALE, RESOLUTION, AND SIGNAL TO NOISE

Brigette A. Martini,[1] Eli A. Silver,[2] and Donald C. Potts[3]

1. INTRODUCTION

This study focuses primarily on the study, monitoring, and hazard evaluation of active volcanic regions using airborne hyperspectral imagery. The age of hyperspectral satellites is now a reality, and as such, it is important to test this technology's strengths and weaknesses as a viable tool in the hands of volcanologists studying active volcanic regions all over the world. Though one satellite (NASA's Hyperion) is now flying, little data has been seen by the scientific community at large. Other hyperspectral satellites have imminent launch dates; however until more space borne data is available, airborne data that approximates space borne instrument characteristics can be used to study volcanic regions of interest. The datasets used in this study image Long Valley Caldera and the Mono-Inyo Volcanic chain located in central-eastern California. The AVIRIS and HyMap data vary in spatial resolution, instrument signal-to-noise ratios and spectral sampling. Though the exact characteristics of various space borne satellites are not matched, they are close enough to draw important conclusions regarding hyperspectral imaging's abilities as a volcanology tool. We compare spatial resolution of the instruments and relate that to the scale of the problems and phenomena being studied.

2. SETTING

Long Valley Caldera formed approximately 760,000 years ago in an eruption that expelled over 600 km^3 of ash and lava (Bailey et al, 1976). Since this event, several successive eruptive events have covered the region with other volcanic flows and domes including the young north-south trending Mono- Inyo volcanic chains that lie in the western caldera. The rhyodacitic stratovolcano Mammoth Mt. is the southernmost volcanic center of the chain. The most recent volcanic activity in the Inyo occurred ~600 years ago and includes phreatic explosion pits on the north flank of Mammoth Mt.

2.1 Hydrothermal system

The hydrothermal system seen today is the vestige of a 40ka peak in activity (Sorey, 1985). Hydrothermal waters in the caldera appear to have a source in the west from a recharge zone at the Sierra front. The waters flow down along range front faults and caldera ring fractures where they are heated by a magmatic source at depth. Transport of these waters appears to be at approximately 1 km depth, along or just within the top of the Bishop Tuff. Temperatures at depth have been directly measured in wells and reached 214°C at one site, though geothermometry suggests source reservoirs reach 240°C (Sorey, 1991). Transport and discharge of these waters then occurs along various fault systems in the western and central caldera. Once at the surface, the hydrothermal waters flow in a plume-like fashion south-eastwards, populating the eastern caldera with a slightly thermal marsh-like environment. Waters are predominantly alkaline in chemistry throughout the caldera and rarely reach boiling. Temperatures range from ~79-93°C in the central hotter regions and cool to 20-25°C in the eastern caldera. Extensive deposits of travertine and sinter can be seen in these areas, though present deposition is primarily travertine (Lipshie, 1976).

[1] Earth Sciences Department, UCSC, bmartini@es.ucsc.edu
[2] Earth Sciences Department, UCSC, esilver@es.ucsc.edu
[3] Ecology and Evolutionary Biology Department, UCSC, potts@biology.ucsc.edu

Hydrothermal alteration products generally consist of argillic phase kaolinite and montmorillinite with localized distributions of alunite and pyrophyllite.

These pools and creeks are characterized by a classic vegetation zonation pattern. The waters themselves are inhabited by an array of thermophilic algae and bacteria. Grasses surround the pools and creeks. The grasses are in turn encompassed by a narrow swath of rabbit brush, which gives way to sagebrush and occasional Juniper trees.

Fumarolic discharge also occurs in several locales around the caldera, most notably along normal faults in Fumarole Valley, formation contacts at Basalt Fumarole, along faults on the flanks of Mammoth Mt. and faults of the Discovery Fault Zone. Advanced argillic alteration predominates locally in these regions exemplified by distributions of the high temperature sulfate alunite surrounded by kaolinite and montmorillinite.

2.2 Structure

Regional structure in eastern California has been largely influenced by Basin and Range extension and Eastern California Shear Zone tectonics. Locally, Long Valley Caldera is bounded on the west by ring fractures and the large northwest trending normal faults of the Sierra Nevada Fault Zone that have experienced up to 2000 meters of normal displacement. Smaller northwest trending normal faults cut the central resurgent dome region while ring fractures rim the eastern boundary of the caldera. On a still smaller scale, the western caldera is populated by northwest trending normal faults, north-south trending normal faults and northeast trending transtensional faults. The intersections of these fault zones result in enhanced vertical permeability. Not only do these intersections serve as foci for movement of hydrothermal waters and zones of discharge, but they also had a profound effect on the formation of the Inyo volcanic chain itself.

2.3 Recent activity

The past 25 years have witnessed a period of elevated unrest for Long Valley including magmatic CO_2 degassing, increased seismic activity, dike intrusions, and re-inflation of the resurgent dome. Such restlessness has led to extensive research and monitoring efforts in Long Valley due to its importance as one the great calderas of the world and its proximity to a major trucking lane (U.S. Highway 395), a major flight route for western U.S. commercial and cargo flights, and several small but tourist laden towns including Mammoth Lakes which sits on the eastern flank of Mammoth Mt. However, though sophisticated suites of geophysical and geochemical studies and monitoring programs have been and are being done in this region, few remote sensing based studies have been completed.

3.0 DATA AND METHODS

The data used in this study consisted of archival AVIRIS images from September 4, 1992, newly acquired AVIRIS data from September 14, 2000, and seven HyMap flightlines from September 7, 1999. The AVIRIS datasets were both taken on the high altitude platform with spatial resolutions of approximately 17-18m while the HyMap data taken from a Cessna aircraft, has a spatial resolution of 3-5m. The two AVIRIS datasets differ primarily in the SNR values reported for each of the two years. Measurements made in the 2.0-2.5 um range only reached a SNR of 100:1 in 1992 data, while 2000 AVIRIS imagery reports a SNR of 400:1 in this same wavelength range. While a higher SNR is ultimately preferable, the study of the capabilities of 1992 AVIRIS data is key for assessing the abilities of spacebased hyperspectral imagery with similar SNR values. For example, the Hyperion sensor reports a SNR of less than 50:1 for the 2.0-2.5 um range.

We compare spatial resolution and bandwidth for the HyMap and two separate AVIRIS flights. The spatial resolution seen in AVIRIS data more nearly approximates spatial resolutions likely available from spacebased hyperspectral sensors such as Hyperion's 30 m pixel. Other sensors such as Orbview-4 (aka Warfighter) have proposed resolution as low as 8m, however such resolutions face political barriers as well as tradeoffs with SNR. The spectral sampling also differs markedly between the two airborne sensors. The 224 band AVIRIS has a fixed bandwidth of 10nm while the 126-band HyMap sensor has variable bandwidths ranging from 13-17nm across the four separate spectrometers. Space borne sensors such as the 220 band Hyperion have bandwidths of 10nm which is similar to AVIRIS.

All analysis in this study was completed within the software program ENVI. The data was atmospherically corrected using ATREM (Gao et al., 1993). Field samples have been taken, and will eventually be used in further calibration efforts. However, analysis to date is performed on data with only the ATREM correction applied. The data was spatially subset to regions of particular interest including sites on Mammoth Mt., a site within the Discovery Fault Zone, and sites at Rhyolite Hot Spring and Little Hot Creek (see Fig. 1). Each subset was divided into visible-near infrared (VNIR) chunks (0.40-1.8um for AVIRIS and 0.45-1.8um for HyMap) and short-wave infrared (SWIR) chunks (2.0-2.5 um for both sensors). The principal components like Minimum Noise Fraction (MNF) algorithm was applied to segregate noise and emphasize signal (Green et al., 1988). Purest pixels are then isolated using the Pixel Purity Index (PPI) and average spectral signatures extracted from these purest pixel classes for use in further classifications. Both the Spectral Angle Mapper algorithm and the Matched Filter algorithm are used in this study and will be discussed individually per study site.

4.0 ANALYSIS

4.1 SNR comparisons at Rhyolite Hot Spring

Rhyolite Hot Spring is an alkaline hot spring located in the central caldera, just to the east of the 300ka Hot Creek rhyolitic lava flow (see Fig. 1). The spring itself is alkaline, discharging at moderate temperatures of 50-55°C. The spring has been modified both by humans (to construct a recreational hot tub), and by livestock. There are two small pools and limited shallow subsurface flow in the region. Though a zone of low discharge presently, this region was home to much higher discharge levels in the past. Just to the southeast of the present-day Rhyolite Hot Spring, is a set of low hills. These hills are extensive travertine terrace deposits formed by paleo-hot springs.

We analyzed subsets covering the Rhyolite Hot Spring area for both 1992 and 2000 AVIRIS imagery. We wanted to see whether mapping in the 1992 imagery would prove to be as successful as mapping efforts in the 2000 imagery. Although the spatial resolutions are the same, the SNR for both images is quite different as detailed previously. After applying the MNF and PPI algorithms, the image-extracted spectral endmembers were used in the Matched Filter algorithm. Figure 2 shows the distribution of four main mineral species: montmorillinite, travertine, Si-bearing mineral (possibly sinter deposits), and kaolinite. Notice first that the scales are a bit different, however, the distribution and character of mineralization in both images are quite similar. These results illustrate that imagery with a medium spatial resolution (17m) and a poor SNR (100:1 in SWIR) is adequate for mapping major mineral assemblages in volcanic environments. Satellite data has poorer resolution (30m) and SNR (50:1) than 1992 AVIRIS; however, results invoke optimism for satellite-based mineral mapping.

4.2 Vegetation and microorganism mapping at Little Hot Creek

Little Hot Creek is located in the east-central caldera on the eastern flanks of the resurgent dome. It is a west to east flowing hot creek that discharges alkaline waters at temperatures near boiling (90-95°C). Discharge is the second highest in the caldera (behind Hot Creek) at 250 l/s (Sorey, 1985). The Little Hot Creek gorge is bounded on either side by Tertiary sediment cliffs, while the floor of the gorge is home to small travertine terraces, and extensive argillic phase hydrothermal alteration. The pools and creeks of the gorge show thermophilic communities of algae and bacteria. Vegetation species zonation is also seen at this hot creek. The pattern seen at Little Hot Creek and at other creeks and pools around the caldera, is outlined in Figure 3. Microorganisms are found in the waters of the creeks and pools. Grasses surround the pools, which are in turn surrounded by a narrow swath of rabbitbrush. The rabbitbrush then grades into sagebrush. The only trees found near the hot creeks are Junipers. Also shown in Figure 3 is a plot of the spectral signatures of communities of cyanobacteria. The presence of such microorganisms may indicate current hydrothermal discharge. Such communities desiccate when water levels drop; however, their spectral signatures remain intact. Thus, their presence indicates that thermal waters have flowed over the surface either presently or in the near past.

The imagery in Figure 4 tries to answer several questions. First, can we map the vegetation zonation patterns shown in Figure 3? Second, what role does spatial resolution and SNR play in such determinations? We attacked these questions by analyzing three different images from three different years and two different sensors. Each image was spectrally subset to include only the VNIR wavelengths. The far left image shows Spectral Angle Mapper (SAM) results for 1992 AVIRIS imagery. Recall, that this data has a 17-18m pixel and a SNR of roughly

400:1 in the VNIR. The image in the middle is 2000 AVIRIS data, also with a 17-18m pixel, but with a SNR of roughly 900:1 in the VNIR. Finally, the image on the far right is HyMap data that possesses a 3-5m pixel and a SNR of roughly 1200:1 in the VNIR.

We find that the zonation pattern can be discriminated in all three datasets, though the HyMap image possesses the most detail, as would be expected from a 5m pixel. The microorganisms map as the red and magenta colors, while the dark greens are likely grasses and the lighter greens are rabbitbrush. Cyan is a mix of sagebrush and soils, while the blues and yellows correspond to sagebrush found along steep slopes in shade. Second, most of the hot pools are not much larger than approximately $100m^2$. The pixels of AVIRIS produce an area of approximately $300m^2$. It is thus impressive that such small features are map-able in data with lower spatial resolution and degraded signal –to-noise (especially that seen in the 1992 AVIRIS). Not all of these results have been field-checked, however the spectral signature for cyanobacteria has a very distinctive geometry and a prominent absorption at 0.62μm due to the pigment phycocyanin. Image extracted signatures from the red and magenta pixels show this 0.62μm feature, and hence likely contain cyanobacteria mats in some proportion. 1992 AVIRIS data is similar to that data expected from such sensors as Hyperion. Hence these results suggest that simple vegetation zonation patterns and communities of thermophilic organisms indicative of hydrothermal discharge may be identifiable from space-based hyperspectral sensors.

4.3 Hydrothermal mineral mapping in the western caldera with AVIRIS and HyMap

Waters in the western caldera are likely heated by a magmatic source at depth beneath the Mono-Inyo volcanic chain. Such waters are known to discharge in the central caldera along northwest-trending normal faults that cut the resurgent dome. The same waters flow along the caldera floor to the east in a spreading hydrothermal plume. In contrast, no surficial discharge of liquid water is known to occur in the topographically higher western caldera, however, extensive hydrothermal alteration is found here. We have shown in previous HyMap-based work, (Martini et al., 2000), that the most extensive and highest temperature alteration in the Long Valley region is found on the flanks of Mammoth Mt., especially the south-western flank. Linear distributions of alteration indicate faults and/or fractures both previously mapped and newly identified. In this study, 2000 AVIRIS imagery was analyzed, and the same distributions and mineral species were found on the flanks of Mammoth as were found in the 1999 HyMap imagery.

Dissimilarities exist as well. The presence of the sulfate alunite along the Discovery Fault Zone to the northeast of Mammoth Mt. had been mapped previously in the HyMap imagery (Martini et al., 2000). Efforts to map the alunite in the AVIRIS imagery were not as successful. Figure 5 shows the distribution of alunite in the HyMap subset (circled for clarity). Notice that in the AVIRIS imagery, three zones of alunite were not identified that were seen in the HyMap data. We believe this is due simply to differences in pixel size. This region of the caldera is highly vegetated with thick stands of conifers; hence the pixels are highly mixed. Even 5m pixels are mixed, but the 17-18m pixels of AVIRIS simply could not see the limited distributions (10-15 HyMap pixels) of alunite in each of the locations found with the HyMap data.

The northeast-trending faults of the Discovery Fault Zone necessitate modified structural models for the caldera and for genesis of the Mono-Inyo volcanic chain (Suemnicht and Varga, 1988). The presence of high temperature alteration on them indicates crustal weakness and hence either faults and/or fractures. Regional eastern California structure is populated with fault patterns similar to those seen spectrally in Long Valley. Though the scale of a feature may be small (such as those alteration patches found in the Discovery Fault Zone), its implications may be large.

5.0 CONCLUSIONS

This study demonstrates the abilities of hyperspectral imaging to map distributions of vegetation and mineralization in Long Valley caldera. The relative effect of variable SNRs and spatial resolutions between data sources have differing levels of importance. Mineralization is mapped similarly in both 1992 AVIRIS (poor SNR) and 2000 AVIRIS (good SNR). Vegetation zonation patterns indicative of hot spring discharge are mapped by all three datasets, although AVIRIS (17-18m) has a poorer spatial resolution than HyMap (3-5m). Finally, alunite mineralization is detected in both AVIRIS and HyMap, although some deposits were ultimately missed by AVIRIS due to its poorer spatial resolution.

SNR is obviously a controlling factor for success in mapping, however the "poor" SNR of 1992 AVIRIS data did not totally hinder mapping efforts. In fact, the mapping success achieved in 1992 data suggests optimism for space-based hyperspectral mapping efforts. Additionally, spatial resolution is clearly important for biological mapping, and can be critical for some geological applications.

6.0 REFERENCES

Bailey, R.A., G.B. Dalrymple, M.A. Lanphere, 1976, "Volcanism, Structure and Geochronology of Long Valley Caldera, Mono County, California," J. Geo. Res., vol. 81, no. 5, pp. 725-743.

Gao, B.C., K.B. Heidebrecht, A.F.H. Goetz, 1993, "Derivation of scaled surface reflectances from AVIRIS data," Rem. Sens. Env., v.44, pp. 165-178.

Green, A.A., M. Berman, P. Switzer, M.D. Craig, 1988, "A transformation for ordering multispectral data in terms of image quality with implications for noise removal," Rem. Sens. Env., v.26, no.1, pp. 65-74.

Lipshie, S.R., 1976, Geologic guidebook to the Long Valley-Mono Craters region, GSUCLA Field Guide 5, Geol. Soc. of Univ. of Calif., Los Angeles, 184 pp.

Martini, B.A., E.A. Silver, D.C. Potts, W.L. Pickles, 2000, "Geological and geobotanical insights into the hydrothermal structure and magmatic systems of a restless caldera using three meter HyMap imagery: LongValley Caldera, California, USA," Proceedings of the Fourteenth International Conference on Applied Remote Sensing, Las Vegas, NV, v.1, pp. 28-35.

Sorey, M.L., 1985, "Evolution and present state of the hydrothermal system in Long Valley Caldera," J. Geo. Res., v.90, no.13, pp.11219-11228.

Sorey, M.L., G.A. Suemnicht, N.C. Sturchio, G.A. Nordquist, 1991, "New evidence on the hydrothermal system in Long Valley caldera, California, from wells, fluid sampling, electrical geophysics, and age determinations of hot-spring deposits," J. of Volc. and Geotherm. Res., v.48, pp. 229-263.

Suemnicht, G.A. and R.J. Varga, 1988, "Basement structure and implications for hydrothermal circulation patterns in the western moat of Long Valley Caldera, California," J. Geo. Res., v.93, pp. 13191-13207.

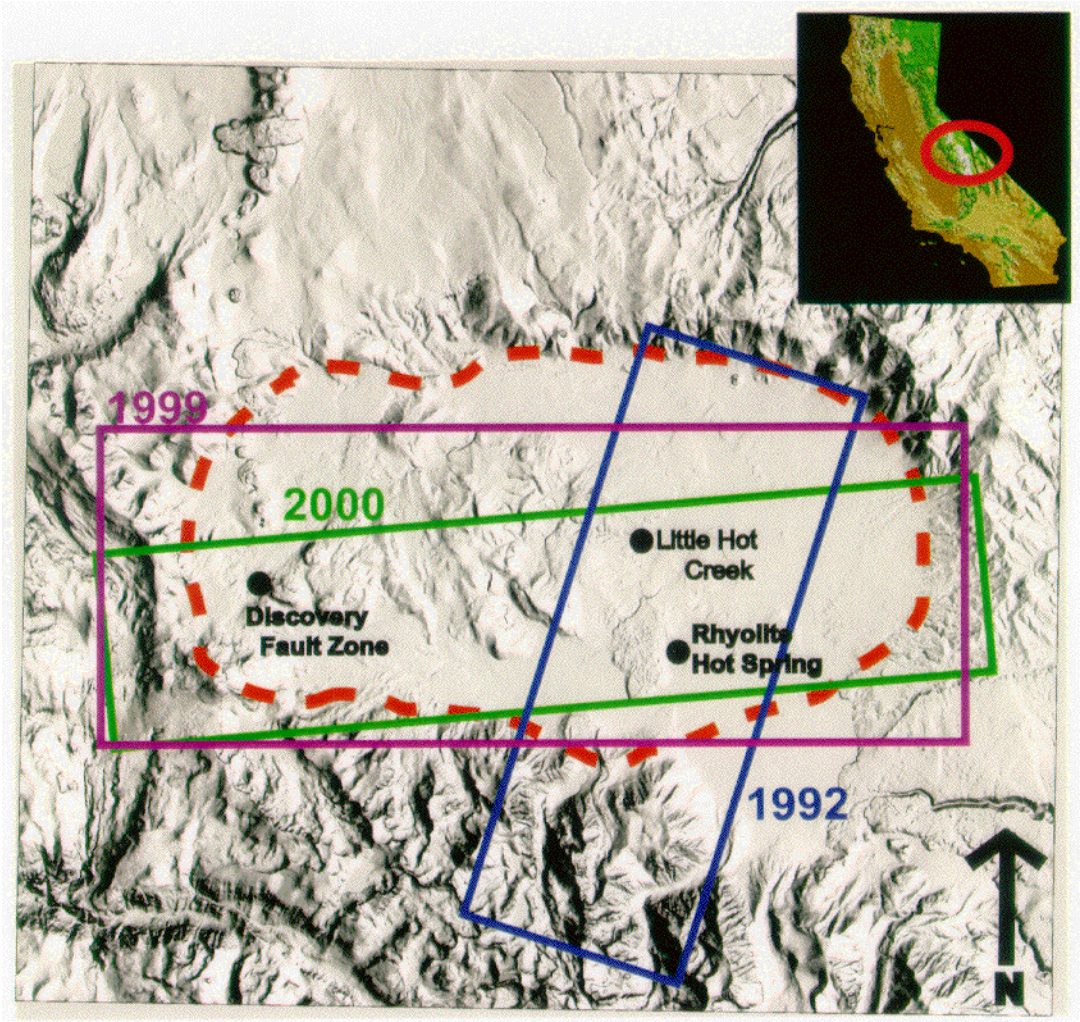

Figure 1. Long Valley caldera outlined in red dashes. The boundaries of the flightlines used in this study shown by rectangles. Specific study sites indicated.

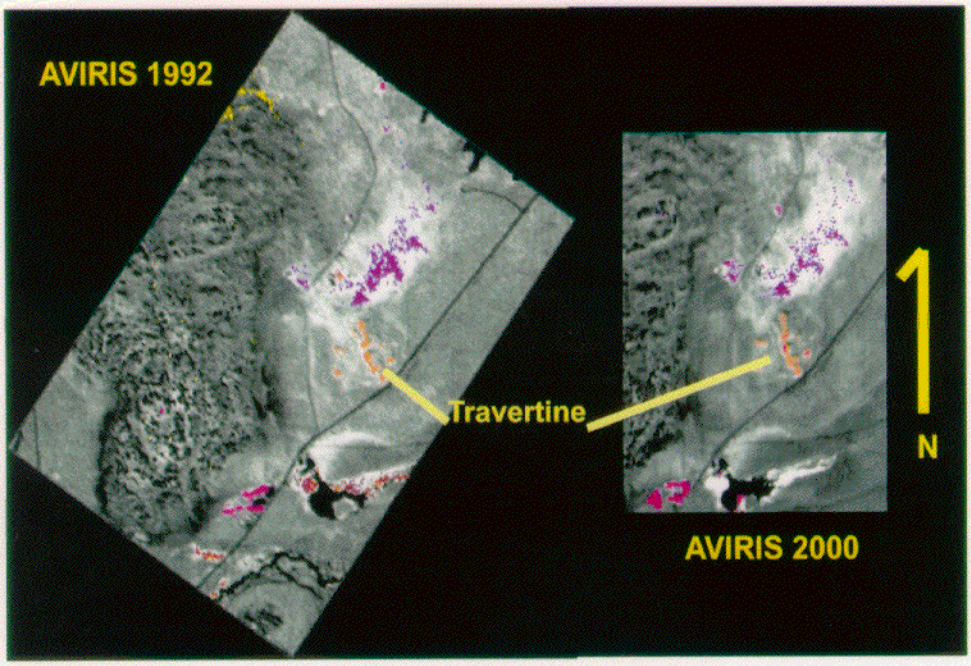

Figure 2. Distributions of mineralization at Rhyolite Hot Springs in the west-central caldera. Classification done in ENVI with Matched Filtering.

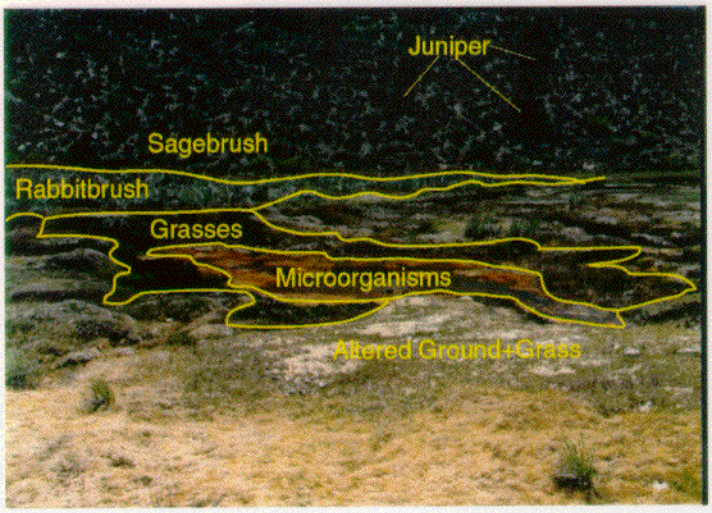

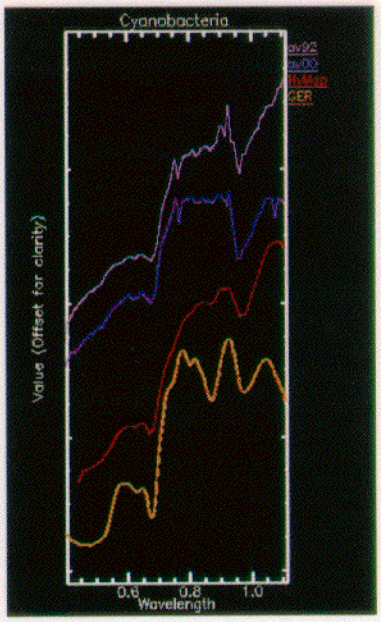

Figure 3. On the right are spectral signatures of microorganisms from each of the datasets, including a GER field spectra. On the left is an image of vegetation zonation patterns found at Little Hot Creek.

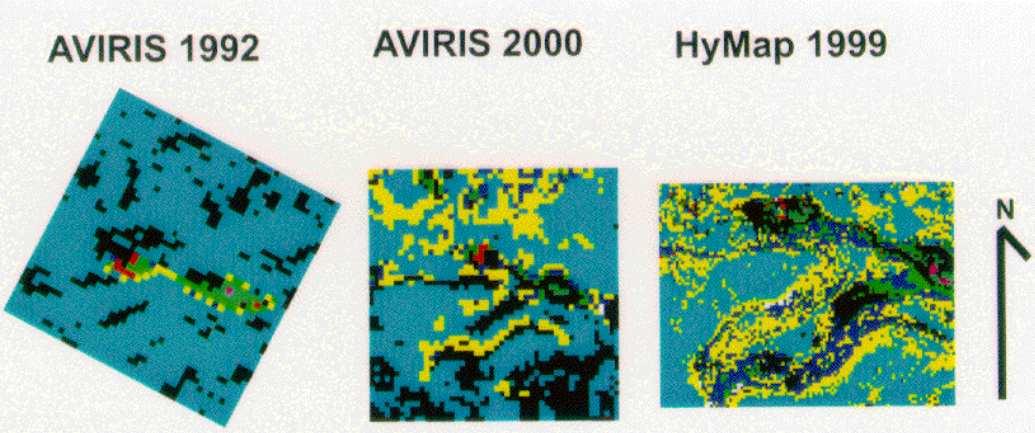

Figure 4. SAM results for both AVIRIS and HyMap data. Differing spatial resolutions, bandwidths, and SNRs effect mapping results. HyMap data clearly has more detail. However, microorganisms in magenta and red map in all three datasets, as well as zonation patterns (albeit crudely in AVIRIS 1992 data).

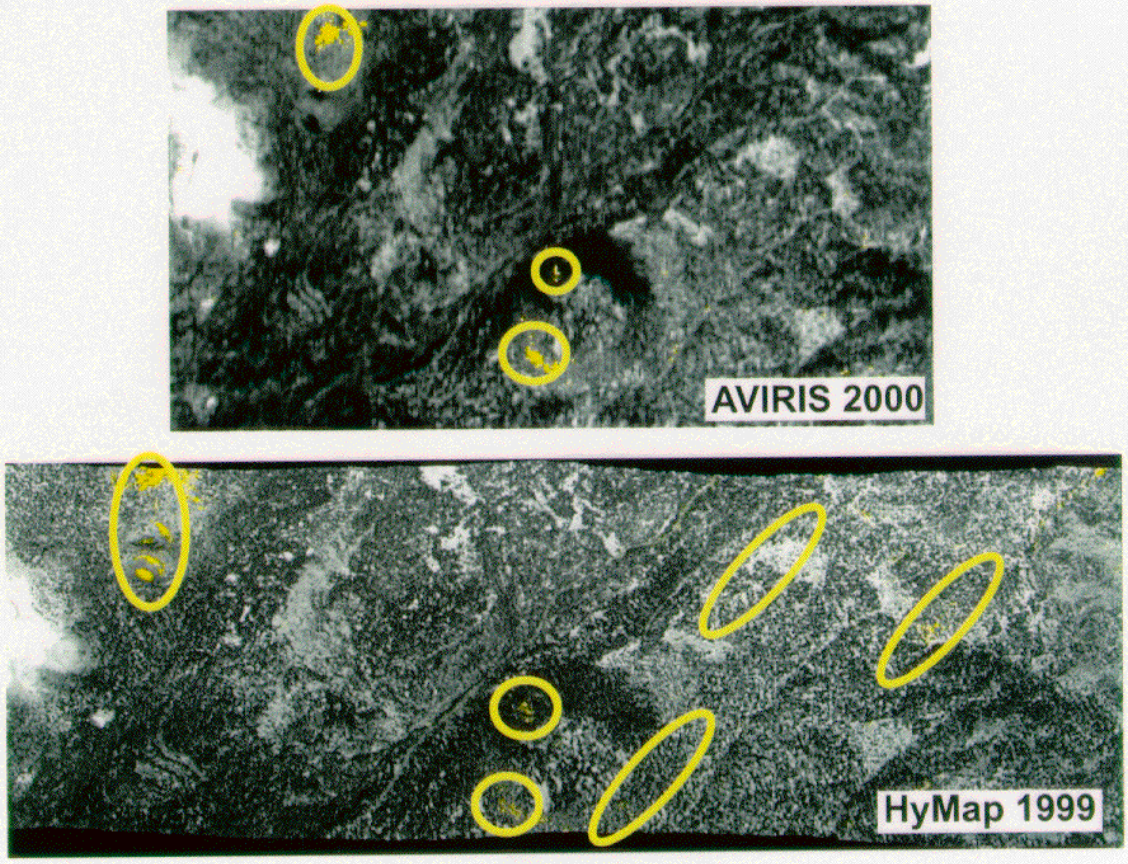

Figure 5. Matched Filter results for AVIRIS and HyMap imagery. Mapped alteration in yellow is alunite. Although the AVIRIS data does reveal alunite, the full distribution is only mapped by HyMap. This is likely due to differences in spatial resolution (17-18m for AVIRIS vs. 3-5m for HyMap).